JOM, Vol. 67, No. 8, 2015
DOI: 10.1007/s11837-014-1266-7

Dielectric and Ferroelectric Behavior of Bismuth-Doped Barium Titanate Ceramic Prepared by Microwave Sintering

A. MAHAPATRA,[1,2] S. PARIDA,[1,3] S. SARANGI,[2] and T. BADAPANDA[1,4]

1.—Department of Physics, C.V. Raman College of Engineering, Bhubaneswar 752054, Odisha, India. 2.—Department of Physics, Centurion University of Technology & Management, Bhubaneswar 751020, Odisha, India. 3.—e-mail: sabyasachiparida023@gmail.com. 4.—e-mail: badapanda.tanmaya@gmail.com

Bismuth-doped barium titanate ceramics with the general formula $Ba_{1-x}Bi_{2x/3}TiO_3$ (x = 0.0, 0.01, 0.025, 0.05) have been prepared by the solid state reaction technique. The phase formation and structural property of all compositions have been studied by x-ray diffraction (XRD) pattern and Rietveld refinement. XRD pattern reports the single phase tetragonal crystal system with space group of *P4mm*. All compositions have been sintered at 1100°C in a microwave furnace for 30 min. The variation of dielectric constant with respect to temperature and frequency was studied and it was found that the dielectric constant decreases whereas transition temperature increased with the increase in Bi content. The diffusivity parameter was calculated by the modified Curie–Weiss law and the diffusivity increased with the increase in Bi content. The ferroelectric property was studied by the P–E hysteresis loop and it was observed that the saturation polarization decreased, but the coercive field increased with Bi content. The optical band gap was calculated from UV–Visible spectroscopy and found to decrease with Bi content.

INTRODUCTION

Ferroelectric materials are of great interest due to their wide application in the electronic industries. Among these, barium titanate, $BaTiO_3$ (BT), a classical perovskite-type compound, has been one of the most studied ferroelectrics over recent decades, not only from the fundamental point of view but also for its industrial applications due to its high dielectric constant, piezoelectric coefficients and high Curie temperature.[1,2] Efforts have been made to improve the dielectric properties by way of controlling grain growth and designing microstructure inhomogeneity. Doping of BT ceramics is very important to obtain the required characteristics for different applications.[3,4] In the ABO_3 perovskite structure, dopant cations can enter substitutionally into two different lattice sites—the smaller, octahedrally coordinated B-sites, or the larger, dodecahedrally coordinated A-sites, mainly depending on their ionic radii.[5–7] The large ionic radius group prefers to incorporate into Ba sites, while the small ionic radius group usually incorporates into Ti sites.[8] For many years, A- and B-site dopants have been used to modify the electrical properties of BT. Substitution of both isovalent and aliovalent cations for the host ones in perovskite lattice plays a very important role in these modification mechanisms.[9] The extent of the solid solution of a dopant ion in a host structure depends on the following: (1) the site where the dopant ion is incorporated into the host structure, (2) the compensation mechanism for the extra charge introduced into the host structure by incorporation of (aliovalent) dopant ions, and (3) the solid solubility limit. Aliovalent cations incorporated in perovskite lattice serve as donors or acceptors, which can affect the electrical characteristics greatly even though the solubility remains at a trace level.[10] Donor dopants have a higher valency than the substituted ions, and therefore their incorporation requires formation of effectively negatively charged defects, e.g., cation vacancies, anion interstitials, electrons, or acceptor impurities.[11–13] There are three possible compensation mechanisms: barium vacancies (V''_{Ba}), titanium vacancies (V''_{Ti}), and electrons (e').[11]

Recently, microwave processing of ceramics has been utilized as an alternative approach for

(Published online December 20, 2014)

conventional sintering of ceramics because of potential advantages such as rapid heating, penetrating radiation, more uniform microstructures and hence higher density.[14–16] The microwave sintering process has unique advantages over the conventional sintering process. The fundamental difference is in the heating mechanism. In conventional heating, elements are transferred to the sample via radiation, conduction and convection and require long duration for sintering the materials which may cause some of the constituents to evaporate, thereby modifying the desired stoichiometry and allowing undesired grain growth. Unlike conventional heating, in microwave heating, the materials themselves absorb microwave energy and then transform into heat within the sample volume and sintering can be completed in shorter times. Though microwave sintering offers several potential advantages, we need to sinter the ceramic samples at a higher temperature in order to achieve good dielectric properties. Major advantages of microwave processing are higher energy efficiency, enhanced reaction and sintering rate and shorter cycle times and cost saving.[17,18] There are few reports on the microwave sintering of some BT-based materials. The microwave sintering of BT-based multilayer ceramic capacitors (MLCC) was reported by Fang et al.[19] Microwave processing of lead-free BT piezoelectric ceramics was investigated by Takahashi et al.[20] But microwave sintering of doped BT has rarely been reported in the literature. So the aim of the manuscript is to study the microstructure and dielectric properties due to substitution of aliovalent Bi^{3+} ions on the Ba^{2+} site of the BT matrix.

EXPERIMENTAL TECHNIQUES

The stoichiometric ratio of starting chemicals $BaCO_3$ (99.9%),TiO_2 (99.9%) and Bi_2O_3 (99.9%) (E.Merck India) were weighed for the composition $Ba_{1-x}Bi_{2x/3}TiO_3$ (x = 0.0–0.1). The weighed powders were ball-milled for 8 h using high-purity Zirconia balls and acetone as a medium. After drying, calculations were done in a high purity alumina crucible at 1100°C for 4 h in a conventional programmable furnace. The phase purity of the calcined powders was confirmed by XRD analysis carried out using a Philips diffractometer model PW-1830 with Cu-K_α (λ = 1.5418 Å) radiation in a wide range of 2θ ($20° < 2\theta < 70°$) at a scanning rate of 2° min^{-1}. The calcined powders were ground by an agate mortar and then pressed into disc form at a pressure of 5 tons using a hydraulic press with 5 wt.% PVA solution added as a binder. The discs were sintered at 1100°C for 30 min in a microwave furnace. For electrical measurements, silver electrodes were applied to the opposite disk faces and were heated at 300°C for 5 min. The frequency (1 kHz–1 MHz) and temperature (30–200°C)-dependent dielectric measurements were carried out using Hioki LCR meter connected to a PC. The ferroelectric hysteresis loop measurement was performed in a P–E loop tracer (Radiant Technologies) based on modified Sawyer–Tower circuit. The UV–vis spectrum was taken using a Shimadzu (UV-2600) spectrophotometer.

RESULTS AND DISCUSSION

X-ray Diffraction and Rietveld Refinement Study

The room temperature Bi-doped BT XRD patterns are shown in Fig. 1. The obtained results reveal that the samples are in a single phase with a tetragonal perovskite structure and have no other peaks of impurities. The observed diffraction peaks of BT phase have been indexed with the database of JCPDS and found to match well with a tetragonal structure (JCPDS Card No. 98-001-3281, PCPDF Card No. 83-1880). The increase of Bi content in the BT lattice promotes a displacement in the XRD peak position at a high angle indicating a decrease in lattice parameter (shown in Table I) and hence the volume of unit cell. This might be due to the substitution of lower ionic radii of Bi^{3+} ion (1.17 Å), which shrinks the unit cell in all three directions decreasing its volume within the same space. Rietveld refinement[21] of the powders has been carried out to confirm these statements. The structural refinement was performed using the Fullprof program.[22] According to the literature,[23] the quality of the structural refinement is generally checked by R values (R_{wp}, R_{Bragg}, R_{exp}, R_p and χ^2). After refinement of these samples, the numbers obtained from R values and χ^2 are recorded (see Table I). They are all consistent with tetragonal structures of space group $P4mm$. However, no structural phase transition has been found in this system to increase the Bi content. The success of a Rietveld refinement is evaluated by the plot difference between observed and calculated patterns (see Fig. 2a–d). The bond lengths of these samples involved in the TiO6 octahedral have been calculated using the Bond_Str program (FullProf suite 2.05) and are given in Table I. It is observed that Ti-O(1) bond length and average Ti-O(2) bond length decrease with increases of Bi content. The displacement of covalent bond O-Ti-O in the perovskite lattice may cause distortions in the [TiO_6] octahedral which is observed at higher compositions of Bi (see Table I). The structural defects observed in the perovskite structure may be attributed to this distortion which may be produced due to the oxygen vacancy in the lattice. That oxygen vacancy may be created by the substitution of trivalent ions (Bi^{3+}) into the Ba^{2+} site. The schematic representation of a unit cell of x = 0.05 ceramic is presented in Fig. 3. The refined structure has been obtained using data given in Table I and the VESTA program (v.3.0 for Windows). In Fig. 3. pink-coloured portions of an atom demonstrate the amount of Bi substitutions in the Ba site.

Dielectric Study

The temperature dependence of dielectric constant (ε') for the $Ba_{1-x}Bi_{2x/3}TiO_3$ samples at 1 kHz, 10 kHz, 100 kHz and 1 MHz are shown in Fig. 4a–d). It is observed from the dielectric study that the maximum dielectric constant decreases with the increase in Bi concentration. Replacing Ba^{2+} by Bi^{3+} results in A-site deficiency to maintain charge neutrality, which increases with an increase in Bi content. Again, the decrement in the lattice parameter shrinks the unit cell which off-centered the Ti^{4+} ion out of the octahedral site so that coupling between the TiO_6 octahedra weakens, which results in a strong decrease in dielectric constant. The shrinkage of the unit cell and weakened TiO_6 octahedral are also presented in the Rietveld refinement analysis.

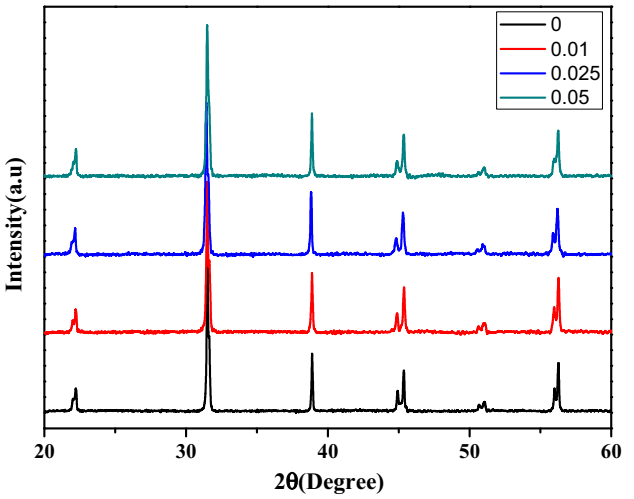

Fig. 1. Room temperature XRD pattern of $Ba_{1-x}Bi_{2x/3}TiO_3$ ceramic.

It is also observed that the transition temperature increases with the increase in Bi content. Aliovalent cations incorporated in the perovskite lattice serve as donors or acceptors, which can greatly affect the electrical characteristics, even though the solubility remains at a trace level.[24] Ohsato et al. have reported that there were three stages of substitution of rare earth elements in BT. In the first stage, Ti ions located on the B site were mainly replaced by rare earth elements, and in the second stage Ba ions on the A site were also mainly replaced by rare earth elements. The third stage was over the limit of substitution and a secondary phase appeared.[25] For the Ba^{2+} heterovalent substitutions by Bi^{3+}, two antagonist effects occur. First, the introduction of Bi^{3+} with its lone pair should give an increase of T_c as was, for instance, the case of Pb^{2+} in $Ba_{1-x}Pb_xTiO_3$.[26] The lone pair effect of Bi^{3+} leads to an increase in the distortion of the octahedron and an increase of T_m, although the cation Bi^{3+} is smaller than Ba^{2+} because of the non-spherical and strongly polarized cation Bi^{3+} (r^{3+} Bi = 1.17 Å in 8 C.N).[27] The second effect is related to the occurrence of cationic vacancies when the large Ba^{2+} is replaced

Table I. Crystallographic data of Ba $_{1-x}Bi_{2x/3}TiO_3$ (x = 0.0, 0.01, 0.025 and 0.05) ceramics obtained using the Rietveld refinement method

$Ba_{(1-x)}Bi_{(2x/3)}TiO_3$	x = 0.0	x = 0.01	x = 0.025	x = 0.05
a (Å)	3.997677	3.994417	3.99217	3.99017
b (Å)	3.997677	3.994417	3.99217	3.99017
c (Å)	4.03554	4.034077	4.033377	4.031077
Volume (Å^3)	64.493667	64.36518	64.281629	64.180618
Structure	Tetragonal	Tetragonal	Tetragonal	Tetragonal
Space group	*P4mm*	*P4mm*	*P4mm*	*P4mm*
x (Ba,Bi)	0	0	0	0
y (Ba,Bi)	0	0	0	0
z (Ba,Bi)	0	0	0	0
x (Ti)	0.5	0.5	0.5	0.5
y (Ti)	0.5	0.5	0.5	0.5
z (Ti)	0.5233	0.51079	0.50808	0.50808
x (O1)	0.5	0.5	0.5	0.5
y (O1)	0.5	0.5	0.5	0.5
z (O1)	0.99958	0.98773	0.92732	0.92712
x (O2)	0.5	0.5	0.5	0.5
y (O2)	0	0	0	0
z (O2)	0.41057	0.44648	0.55859	0.5495
R_{Bragg}	8.757	8.756	8.031	5.756
R_p	32.5	40.9	39.6	38
R_{wp}	32.7	39	37.3	35
R_{exp}	19.17	30.64	28.43	28.31
χ^2	2.9	1.62	1.72	1.53
d Ti-O1 (Å)	1.92205	1.92404	1.6899	1.68918
d Ti-O2 (Å)	2.04996	2.01398	2.00666	2.00206

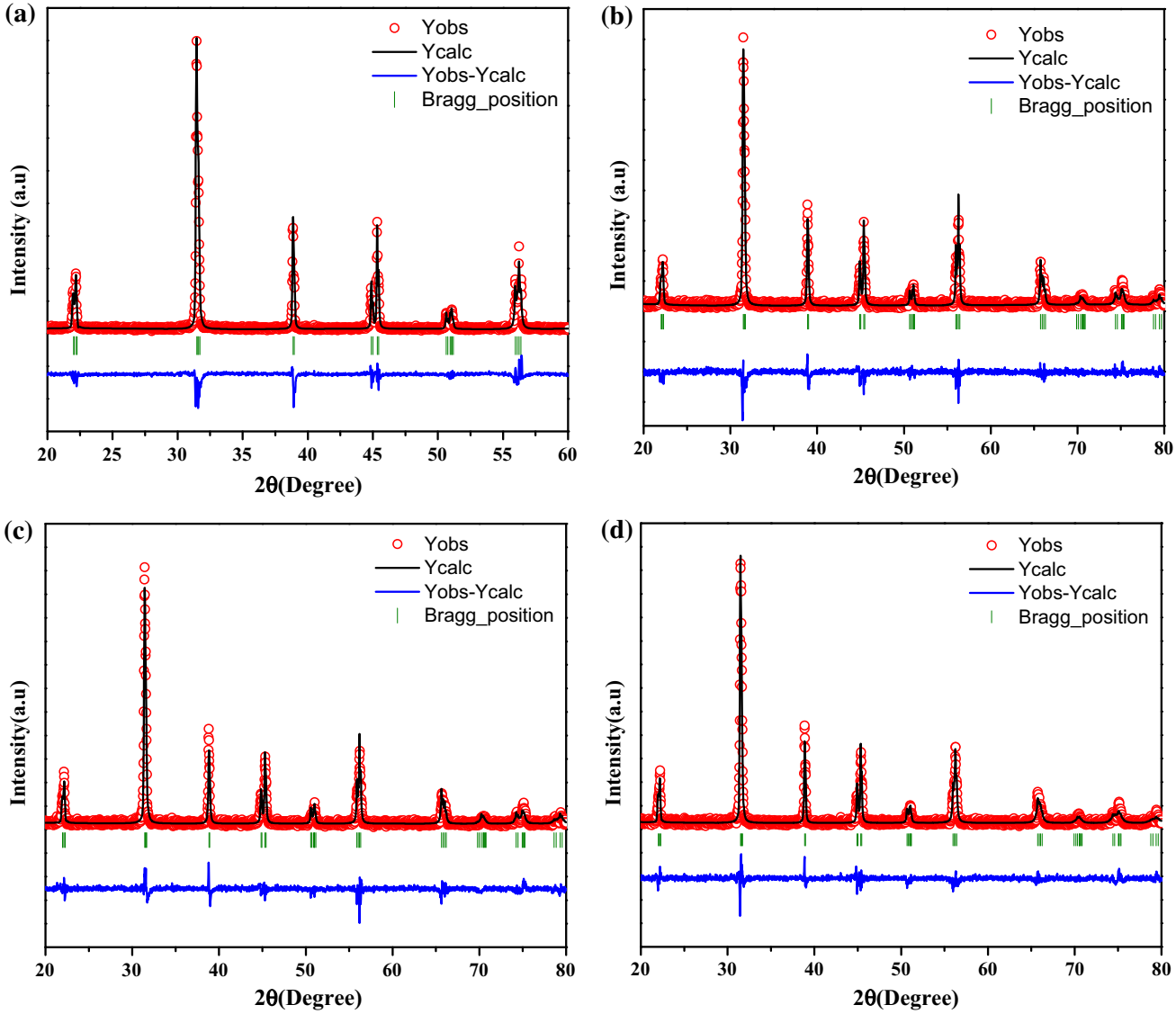

Fig. 2. a–d Rietveld refinement of $Ba_{1-x}Bi_{2x/3}TiO_3$ ceramic (a) $x = 0.0$, (b) $x = 0.01$, (c) $x = 0.025$, and (d) $x = 0.05$.

by the smaller Bi^{3+} leading to a decrease of T_m. Similar kinds of results are obtained in Bi-doped $BaZr_{0.3}Ti_{0.7}O_3$ ceramics.[28] At a higher concentration ($x = 0.05$) of Bi, there is very small variation in the transition temperature. It was observed from x-ray diffraction that there is a slight hint of a secondary phase at $x = 0.05$ which may hinder the further phase formation (see Fig. 1). This phase indicates that at higher concentration ($x = 0.05$), Bi^{3+} tends to occupy B-sites rather than A-sites. The transition can compensate both the lattice stress and the charge imbalance generated at this stage. As a result, the concentration of oxygen vacancies is decreased. The lattice distortion is moderated and the spontaneous polarization is also partially recovered. The Curie temperature exhibits a constant value at about $x = 0.05$ which might correspond to the coexistence of the two substitution modes.

It is also observed from the temperature-dependent dielectric study that the phase transition becomes more diffused with an increase in Bi content. The diffuseness of a phase transition was studied by the modified Curie–Weiss law as

$$\frac{1}{\varepsilon} - \frac{1}{\varepsilon_m} = \frac{(T - T_m)^{\gamma}}{C_1} \quad (\text{at } T > T_m), \tag{1}$$

where γ and C' are assumed to be constants. The parameter γ gives information on the character of the phase transition; for $\gamma = 1$, a normal Curie–Weiss law is obtained, while for $\gamma = 2$, it reduces to the quadratic dependency which describes a complete diffuse phase transition. The plot of log $(1/\varepsilon' - 1/\varepsilon_m)$ versus $\log(T - T_m)$ at different frequencies is shown in Fig. 5, and a linear relationship is observed, in which the diffusivity increases with the

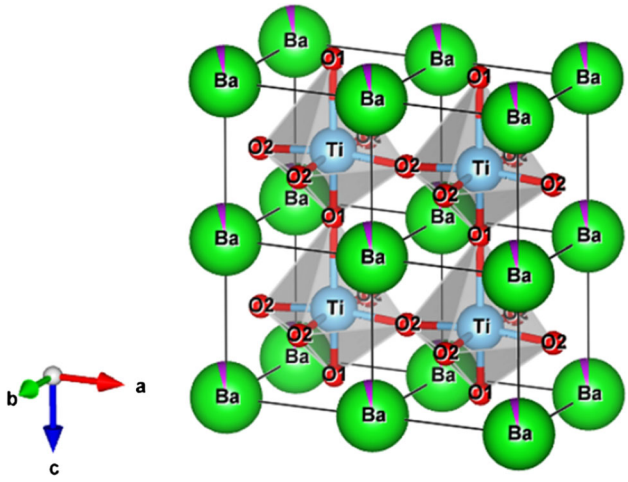

Fig. 3. Schematic representation of $Ba_{1-x}Bi_{2x/3}TiO_3$ unit cell with the tetragonal structure of $x = 0.05$ composition illustrating the $[TiO_6]$ octahedral.

increase in Bi content. The broadness or diffusiveness occurs mainly due to compositional fluctuation and structural disordering in the arrangement of cations in one or more crystallographic sites of the structure.

The substitution of Bi^{3+} for Ba^{2+} will take place according to the Kroger–Vink notation, as follows:

$$Bi_2O_3 \rightarrow 2Bi^{\bullet}_{Ba} + V''_{Ba} + 3O^{x}_{O}, \qquad (2)$$

where Bi and Ba stand for a bismuth atom on the barium site with one positive charge, V''_{Ba} for a barium vacancy with two negative charges and O^{x}_{O} for a neutral oxygen atom on an oxygen site. Thus, the addition of Bi_2O_3 in the BT-based ceramics leads to the formation of a barium vacancy by a charge compensation mechanism. For every two Bi^{3+} substituting ions ($Bi^{\bullet}_{Ba}$), only one A-site vacancy (V''_{Ba}) is created, which produces compositional fluctuation on a microscopic scale. In the same way, the presence of Bi^{3+} ions at the A-site and their

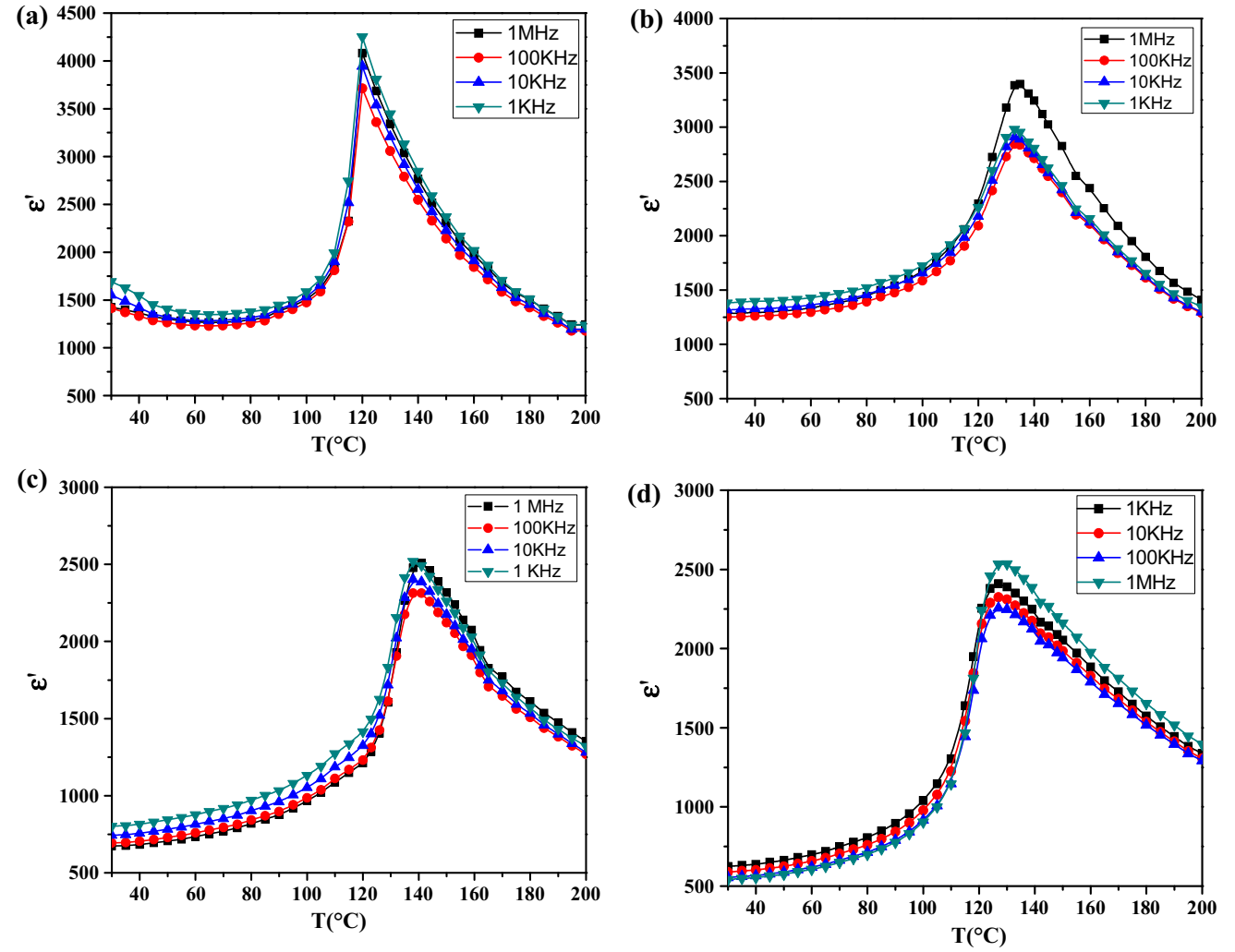

Fig. 4. a–d Dielectric constant (ε') as function of temperature (T) at different frequencies for $Ba_{1-x}Bi_{2x/3}TiO_3$ ceramics (a) $x = 0.0$, (b) $x = 0.01$, (c) $x = 0.025$, and (d) $x = 0.05$.

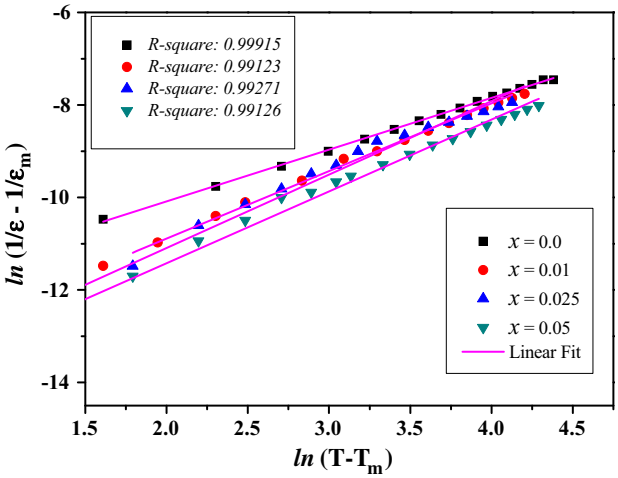

Fig. 5. $\ln(1/\varepsilon - 1/\varepsilon_m)$ versus $\ln(T - T_m)$ of $Ba_{1-x}Bi_{2x/3}TiO_3$ ceramic at 100 kHz.

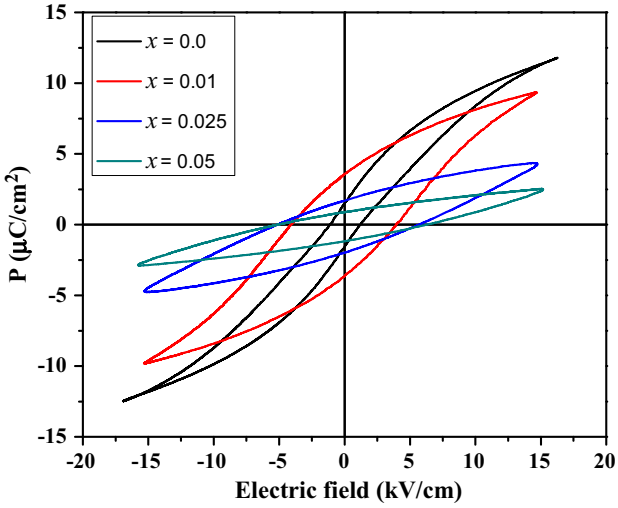

Fig. 6. P–E hysteresis loop of $Ba_{1-x}Bi_{2x/3}TiO_3$ ceramic.

Table II. Parameters obtained from temperature dependent dielectric studies at 100 kHz on the composition of $Ba_{1-x}Bi_{2x/3}TiO_3$ ceramics with different Bi content

Composition $Ba_{(1-x)}Bi_{(2x/3)}TiO_3$	ε_m	T_m (°C)	γ	E_c (kV/cm)	P_r (μC/cm^2)
x = 0.0	3712.429	120	1.12	1.10	1.41
x = 0.01	2843.999	133	1.46	4.08	3.56
x = 0.025	2312.655	138	1.55	5.29	1.71
x = 0.05	2256.176	127	1.58	4.96	0.9

interaction with A-site vacancies give rise to a lattice distortion. The lattice distortion and the compositional fluctuation originating from $Bi^{\bullet}_{Ba}$ and V''_{Ba} inclusions in the BT structure may explain the diffusion of the ferroelectric phase transition. Again, $Bi^{\bullet}_{Ba}$ and V''_{Ba} increase with the increase of Bi^{3+}, and for this reason the compositional inhomogeneity is enhanced. As a consequence, the increase of Bi content enlarges the degree of diffuseness as observed experimentally.

The diffuse phase transition behavior as observed in this ceramic can be induced by many factors, such as microscopic composition fluctuation, the merging of micropolar regions into macropolar regions, or a coupling of the order parameter and local disorder mode through the local stream. Vugmeister and Glinchuk reported that the randomly distributed electrical strain field in a mixed oxide system is the main reason leading to the diffuse behavior.[29] As no macroscopic phase separation exists in the studied ceramics, we cannot exclude chemical heterogeneity at a nanoscale. The distortion arising in the oxygen octahedra, a redistribution of the charge, and local formation of charge center results may be the sources of the random field. This kind of random field is much weaker than that stemming from heterovalent cation substitution as in conventional ferroelectrics. Hence, at high temperature, the strength of random field-fluctuating dipole moments of the individual unit cell can give rise to polar nanoregions. Here, the polar correlations are strongly diminished and polar domains are less likely to nucleate. The bismuth substitution not only decreases the grain size but also the size and distribution of the polar regions. This can lead to the broadening of relaxation time and significant improvement of the diffusion properties of Bi-doped BT ceramics.

Figure 6 shows the ferroelectric hysteresis loop of Bi-doped BT ceramics obtained under a maximum applied electric field of 20 kV/cm. The P–E loops for all the compositions are recorded at room temperature and at a frequency of 100 Hz. The values of remnant polarization (P_r) and coercive field (E_c) are listed in Table II. It can be seen that both increase with the increase in Bi content. The increase in the coercive field indicates that the material gets harder. The highest value of P_r is observed at x = 0.01, but with further addition of Bi, the P_r value decreases. Decreases in P_r in higher compositions may be due to the increase in the concentration of oxygen vacancies in the system. And, as a result, the domain pinning effect is increased.

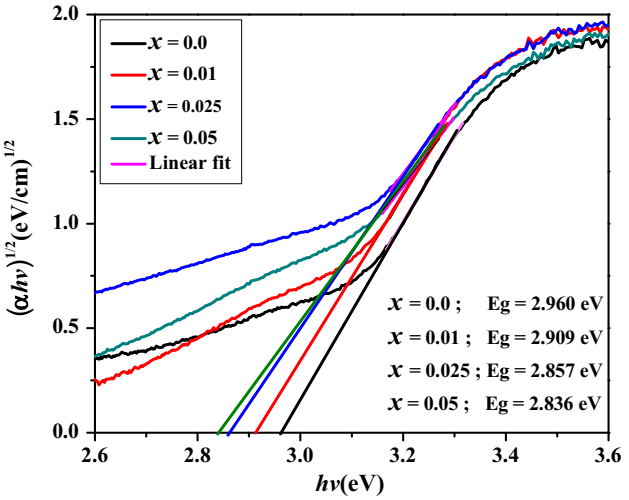

Fig. 7. The UV–vis absorbance spectrum of $Ba_{1-x}Bi_{2x/3}TiO_3$ ceramic.

Optical Study

Figure 7 shows the UV–vis absorbance spectrum of Bi-doped BT ceramic. The optical band gap energy (E_g) was estimated by the method proposed by Wood and Tauc.[30] According to these authors, the optical band gap is associated with the observance and photon energy by the following equation:

$$h\nu\alpha \propto (h\nu - E_g ap)^n, \tag{3}$$

where α is the absorbance, h is the Planck constant, ν is the frequency, E_g is the optical band gap, and n is a constant associated with the different types of electronic transitions (n = 1/2, 2, 3/2 or 3 for direct allowed, indirect allowed, direct forbidden and indirect forbidden transitions, respectively). Thus, the E_g value of $Ba_{1-x}Bi_{2x/3}TiO_3$ ceramic was evaluated by extrapolating the linear portion of the curve or tail. In our work, the UV–vis absorbance

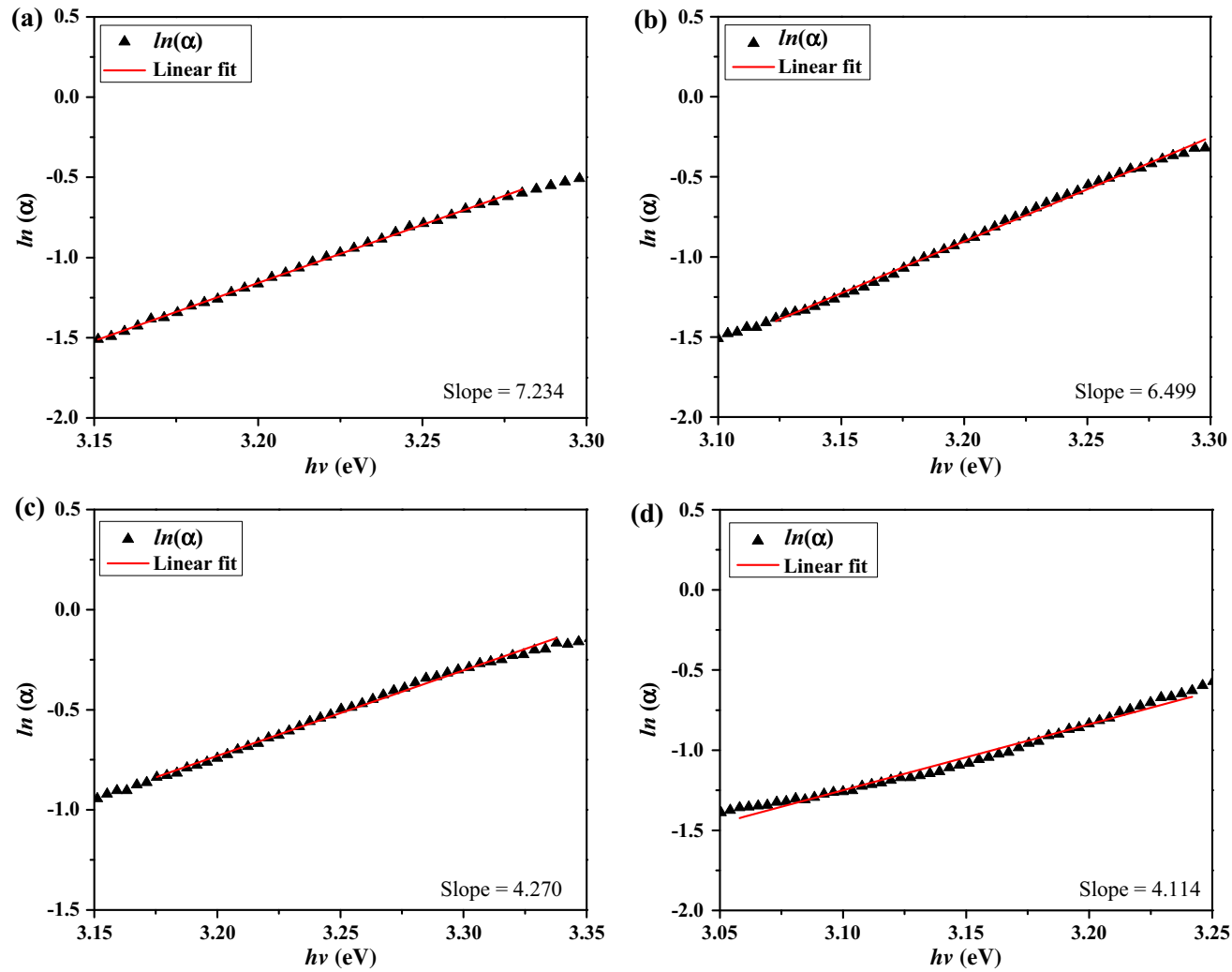

Fig. 8. a–d Plot of lnα vs. $h\upsilon$ for the determination of Urbach energy (E_u) for $Ba_{1-x}Bi_{2x/3}TiO_3$ ceramic (a) x = 0.0, (b) x = 0.01, (c) x = 0.025, and (d) x = 0.05.

spectrum suggests an indirect allowed transition and, therefore, the $n = 2$ was used in Eq. 3.

The literature[31] describes that the band gap energy is indirect when the electronic transitions occur from maximum-energy states located near or in the valence band (VB) to minimum-energy states below or in the conduction band (CB), but in different regions in the Brillouin zone. The distinct E_g calculated from the UV–vis absorption (Fig. 7) spectra indicated the existence of intermediary energy levels within the optical band gap. It is possible to conclude that these energy states are basically composed of O 2p orbitals (near the VB) as well as Ti 3d orbitals.[32] The origin of these orbitals or energy levels is directly related to the presence of structural order–disorder into the random lattice, as a consequence of distortions on the [TiO_6] clusters.[33]

The obtained E_g values for the doped ceramics can be associated with the structural disorder introduced into the lattice due to creation of A-site vacancies and distortions in the [TiO_6] clusters. A-site vacancies introduce shallow defects in the band gap of BT, decreasing the value. Vacancies increase with the increase in Bi content and this results in the formation of larger numbers of shallow defects. Distortion in the TiO_6 octahedron also increases and hence the band gap decreases further.[34]

The width of defect bands formed in the band gap can be determined. These defect band states create a band tail extending from the lower of CB to deep down in the band gap, and, similarly, the defect states very near to the VB also spread the VB edge deep inside the gap. As a result, on both sides of the VB maximum and the CB minimum, an energy tail is formed and the banding of tail is associated with the disorders present in the system. This defect tail is known as the Urbach tail, and the energy associated with this defect tail is referred to as Urbach energy.[35,36] The equation of Urbach energy is given by $\alpha = \alpha_o \exp\left(\frac{E}{E_U}\right)$ where $E = h\upsilon$, where α is the absorption coefficient and E_U is the Urbach energy.[37] Since the absorption coefficient is proportional to absorbance,[38] therefore in general we can write $\alpha \sim e^{\frac{E}{E_U}}$. The Urbach energy is calculated by plotting lnα versus photon energy ($h\upsilon$). The reciprocal of the slope of linearly fitted lines gives the value of Urbach energy as per the equation:

$$\ln(\alpha) = C + \frac{E}{E_U} \tag{4}$$

The plots for Urbach energy calculation are shown in Fig. 8a–d. From Fig. 9, it can be observed that as the band gap decreases, the magnitude of defect energy (Urbach energy) increases. This clearly indicates that sub-band states formed in between the valence and CBs result in the narrowing of the band gap. The effective reduction of the band gap of $Ba_{1-x}Bi_{2x/3}TiO_3$ powders with an increase of doping level signifies that the number of defect levels below the CB increases to such an extent that the band edge is shifted deep into the forbidden gap. A similar type of behavior is observed in Cu-doped TiO_2 nano-particles.[37]

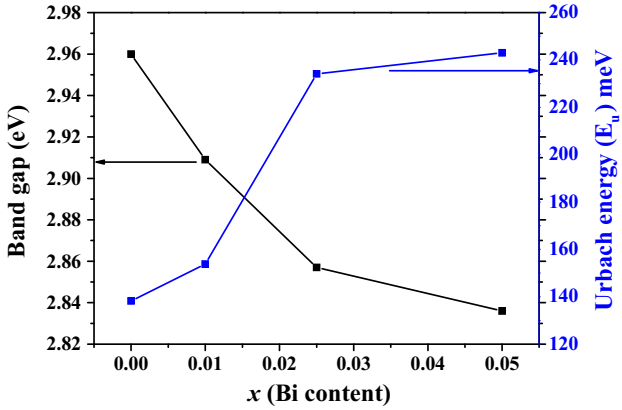

Fig. 9. Variation of band gap (E_g) and Urbach energy (E_u) for different concentrations of Bi.

CONCLUSION

Bismuth-modified BT ceramics have been prepared by the solid state reaction route. The x-ray diffraction study and Rietveld refinement study show that all the composition possess a single phase tetragonal crystal system with the space group of *P4mm*. The dielectric constant decreases with the increase in Bi content which may be due to the incorporation of a smaller ionic radius which causes lattice parameter transformation and internal stress. The increase in the transition temperature in the temperature-dependent dielectric study is due to the enhancement in the tetragonality with Bi doping. The diffusivity value is calculated from a modified Curie–Wiess law and found to increase with the increase in Bi content. The ferroelectric hysteresis loop shows an increment in remnant polarization and coercive fields. The increase of oxygen vacancies due to the incorporation of Bi^{3+} content into the BT lattice causes a decrease of the band gap. Values of the Urbach tail are found to increase with Bi^{3+} doping which confirms that crystal disorder increases due to defects or impurity. This structural distortion and/or defects in the band gap raise a fundamental condition for the existence of polarizations and PL emissions. Finally, it can be concluded that the increase of Curie temperature and dispersive characteristics of the transition temperature are suitable for high-temperature capacitance stability of MLCs.

REFERENCES

1. S. Fujishima, *IEEE Trans. Ultrason. Ferroelectr. Freq. Control* 47, 1 (2000).
2. G.H. Haertling, *J. Am. Ceram. Soc.* 82, 797 (1999).
3. S.P. Feofilov, A.A. Kaplyanskii, A.B. Kulinkin, and R.I. Zakharchenya, *J. Lumin.* 129, 1689 (2009).

4. H. Kishi, N. Kohzu, J. Sugino, H. Ohsato, Y. Iguchi, and T. Okuda, *J. Eur. Ceram. Soc.* 19, 1043 (1999).
5. M. Ganguly, S.K. Rout, T.P. Sinha, S.K. Sharma, H.Y. Park, C.W. Ahn, and I.W. Kim, *J. Alloys Compd.* 579, 473 (2013).
6. S.K. Ghosh, M. Ganguly, S.K. Rout, S. Chanda, and T.P. Sinha, *Solid State Sci.* 30, 68 (2014).
7. S. Mahboob, A.B. Dutta, C. Prakash, G. Swaminathan, S.V. Suryanarayana, G. Prasad, and G.S. Kumar, *Mater. Sci. Eng., B* 134, 36 (2006).
8. B.D. Stojanovic, Advanced in sintered electronic materials.*Proceedings of the Ninth World Round Table Conference on Sintering*, ed. B.D. Stojanovic, V.V. Skorokhod, and M.V. Nikolic (New York: Kluwer, 1999), p. 367.
9. Y. Tsur, T.D. Dunbar, and C.A. Randall, *J. Electroceram.* 7, 25 (2001).
10. M.T. Biscaglia, V. Buscaglia, M. Viviani, P. Nanni, and M. Hanuskova, *J. Eur. Ceram. Soc.* 20, 1997 (2000).
11. H.M. Chan, M.P. Harmer, and D.M. Smyth, *J. Am. Ceram. Soc.* 69, 507 (1986).
12. A.S. Shaikh and R.W. Vest, *J. Am. Ceram. Soc.* 69, 689 (1986).
13. D.K. Hennings, B. Schreinemacher, and H. Schreinemacher, *J. Eur. Ceram. Soc.* 13, 81 (1994).
14. C.-T. Hu, H.-W. Chen, H.-Y. Chang, and I.-N. Lin, *Jpn. J. Appl. Phys.* 37, 186 (1998).
15. E.T. Thostenson and T.-W. Chen, *Composites A.* 30, 1055 (1999).
16. D. Agrawal, J. Cheng, Y. Fang, and R. Roy, *Microwave Processing of Ceramics, Composites and Metallic Materials*, ed. D.E. Clark, D.C. Folz, C.E. Folgar, and M.M. Mahmoud (American Ceramic Society Publication, Weterviller, 2005), p. 205.
17. M. Oghbaei and O. Mirzaee, *J. Alloys Compd.* 494, 175 (2010).
18. R. Angalakurthi and K.C. James Raju, *IOP Conf. Ser. Mater. Sci. Eng.* 18, 092028 (2011).
19. Y. Fang, M.T. Lanagan, D.K. Agrawal, G.Y. Yang, C.A. Randall, T.R. Shrout, A. Henderson, M. Randall, and A. Tajuddin, *J. Electroceram.* 15, 13 (2005).
20. H. Takahashi, Y. Numamoto, J. Tani, K. Matsuta, J. Qiu, and S. Tsurekawa, *Jpn. J. Appl. Phys.* 45, L30 (2006).
21. H.M. Rietveld, *Acta Crystallogr.* 22, 151 (1967).
22. Fullprof 2000, version July 2001. Juan Rodríguez-Carvajal, Laboratoire Léon Brillouin (CEA-CNRS) CEA/Saclay, Gif sur Yvette Cedex.
23. M. Ferrari and L. Lutterotti, *J. Appl. Phys.* 76, 7246 (1994).
24. K. Watanabe, H. Ohsato, H. Kishi, Y. Okino, N. Kohzu, Y. Iguchi, and T. Okuda, *Solid State Ionics* 108, 129 (1998).
25. C. Ostos, L. Mestres, M.L. Martnez-Sarrión, J.E. Garca, A. Albareda, and R. Perez, *Solid State Sci.* 11, 1016 (2009).
26. Landolt-Börnsteidn III, *Ferroelectric and Related Substances*, vol. 16 (Berlin: Springer, 1981).
27. R.D. Shannon, *Acta Crystallogr. A* 32, 751 (1976).
28. A. Kerfah, K. Taïbi, A. Guehria-Laidoudi, A. Simon, and J. Ravez, *Solid State Sci.* 8, 613 (2006).
29. B.E. Vugmeister and M.D. Glinichuk, *Rev. Mod. Phys.* 62, 993 (1990).
30. D.L. Wood and J. Tauc, *Phys. Rev. B.* 5, 3144 (1972).
31. L.S. Cavalcante, M.F.C. Gurgel, E.C. Paris, A.Z. Simões, M.R. Joya, J.A. Varela, P.S. Pizani, and E. Longo, *Acta Mater.* 55, 6416 (2007).
32. M. Anicete-Santos, L.S. Cavalcante, E. Orhan, E.C. Paris, L.G.P. Simões, M.R. Joya, I.L.V. Rosa, P.R. de Lucena, M.R.M.C. Santos, L.S. Santos-Júnior, P.S. Pizani, E.R. Leite, J.A. Varela, and E. Longo, *Chem. Phys.* 316, 260 (2005).
33. C. Laulhé, F. Hippert, R. Bellissent, A. Simon, and G.J. Cuello, *Phys. Rev. B.* 79, 064104 (2009).
34. M.L. Moreira, M.F.C. Gurgel, G.P. Mambrini, E.R. Leite, P.S. Pizani, J.A. Varela, and E. Longo, *J. Phys. Chem. A* 112, 8938 (2008).
35. M. Borah and D. Mohanta, *J. Appl. Phys.* 112, 124321 (2012).
36. H. Moulkia, S. Hariech, and M.S. Aida, *Thin Solid Films* 518, 1259 (2009).
37. B. Choudhury, M. Dey, and A. Choudhury, *Int. Nano Lett.* 3, 25 (2013).
38. N. Kumari, A. Ghosh, S. Tewari, and A. Bhattacharjee, *Indian J. Phys.* 88, 65 (2014).